Constructing a Simple Hybrid Model of Perineural Invasion

Jeremy P D'Silva and Marisa C. Eisenberg
University of Michigan, Ann Arbor

Abstract

1 Introduction

Head and neck squamous cell carcinoma (HNSCC) is the sixth most common cancer worldwide, with a five-year survival rate of approximately 50% [1, 2]. This underscores the need for further study into the mechanisms that contribute to HNSCC progression, including invasion, metastasis, and recurrence.

One mechanism of invasion of HNSCC is perineural invasion (PNI). PNI is defined broadly as, "invasion in and about nerves by cancer..." [3], and more specifically as, "tumor cells within...the nerve sheath or tumor foci outside of the nerve with involvement of 33% of the nerve's circumference" [4]. PNI involves complex interactions between cancer and nerves. A combination of signaling molecules and other micro-environmental factors promotes tropism of cancer towards the nerve [5]. Moreover, recent research has proven the previously hypothesized idea that cancer stimulates neurite outgrowth: the nerve sends neurites toward the cancer, which promotes invasion in *in vivo* models [6]. This process can be compared to angiogenesis, wherein via VEGF and other signalling molecules, a tumor can promote the growth of endothelial cells, and ultimately vasculature, towards the tumor.

Recent work [6] has validated the analogous mechanism for HNSCC *in vivo*, using an experimental model setup based on a chick chorioallantoic membrane (CAM) experimental model. In this process, injury, inflammation, or cytokine release leads to galanin (Gal) secretion by nerve. Then, Gal reaches the tumor, where it is sensed by Galanin receptor 2 (GalR2), a G-protein-coupled receptor. Through a signal transduction pathway, this leads to NFATC2-mediated transcription of the genes coding for Gal and Cox2. Cox2 is an enzyme that catalyzes the formation of PGE2;

PGE2 and Gal are made and secreted by the tumor. Gal secreted by the tumor promotes neurite outgrowth from the nerve, and PGE2 promotes a more invasive tumor phenotype. This facilitates PNI.

This mechanism was studied *in vivo* in the chick corioallantoic membrane (CAM) experimental model [6]. In these experiments, cancer cells, representing a tumor, are added onto the collagenous basement membrane of the chick egg. A rat dorsal root ganglion is implanted into the connective tissue underneath the basement membrane. The neural tissue and cancer cells can be labeled and imaged to visualize and quantify the extent of neurite outgrowth and cancer invasion.

Although many mathematical models have been developed for angiogenesis (for reviews see [7, 8]), few mathematical models exist for PNI. In particular, there is a need for mathematical models of PNI that take into account the geometry and spatial dynamics of invasion, as indicated by Lolas and co-authors, who highlight that need in their paper on a deterministic mean-field model for cancer-induced neurite outgrowth [9]. Their model tracks concentrations of different cell types to model the cancer-nerve interaction without a spatial component.

We developed a hybrid model for the neurite outgrowth in PNI. Hybrid models combine deterministic components, in this case, PDEs governing diffusion of signalling molecules, with stochastic agent-based models, in this case, governing neurite outgrowth. Previous hybrid models, upon which our model is based, have been successful in capturing the phenotypes and mechanisms underlying angiogenesis [10, 11]. We calibrated our model to the results obtained in the CAM *experimental model*. Our model captured the patterns of neurite outgrowth observed *in vivo* by Scanlon and co-authors [6] in the CAM experiments. Based on our model, we characterize a "chemotactic regime", a region around a tumor where neurites are able to sense the tumor based on the local amount and gradient of galanin.

2 Methods

2.1 Mathematical model formulation

The mathematical model is a hybrid model, consisting of a PDE to describe the diffusion and decay of Gal and a stochastic agent-based model (ABM) for neurite outgrowth.

2.1.1 Galanin submodel

The diffusion and decay of Galanin are modeled by:

$$\frac{\partial G}{\partial t} = \nabla \cdot (D \nabla G) - aG \tag{1}$$

where G is the concentration of Gal, D is the diffusion constant of Gal, and a is the decay rate of Gal. The spatial domain for the PDE is a two-dimensional rectangular section of the real plane with "holes" representing the tumor and the nerve cell body. The boundary conditions are no-flux around the outer edges of the domain and the boundary conditions around the tumor and nerve have flux, to represent secretion rates of Gal from each entity. The time-dependent PDE was solved numerically over time in MATLAB using PDE Toolbox, which uses a finite element method. The domain was triangulated with the PDE Toolbox's default triangulation function. The function value and gradient vectors at specific points were determined via the functions evaluateGradient and interpolateSolution.

The PDE model was solved in increments of $\frac{10}{3}$ minutes for 1 hour, on a 3 cm * 3 cm domain. The gradient and amount of galanin were interpolated on a 601-by-601 square lattice of side length 600 μm, centered around the origin. The neurites and cancer were placed within this sub-space. After 1 hour of simulation, the boundary condition representing tumor secretion was recalculated, and the solution from the previous time-step was used as the initial condition for the next hour of solving the PDE.

The boundary condition representing tumor secretion of galanin is a function of the amount of galanin at the boundary of the tumor, at the point nearest the nerve. The functional form is logarithmic, in order to include a "saturation effect", so that the secretion rate of the tumor stays within a plausible biological maximum bound and does not blow up.

2.1.2 Neurite submodel

We developed a stochastic ABM to model the outgrowth of neurites. Neurites grow by elongation of cytoskeletal structures, based on intracellular signalling as well as external cues. The neurite tip contains many receptors that can sense external ligands and gradients, including extracellular matrix-bound and freely diffusing ligands. In response to these external signals, the neurite can

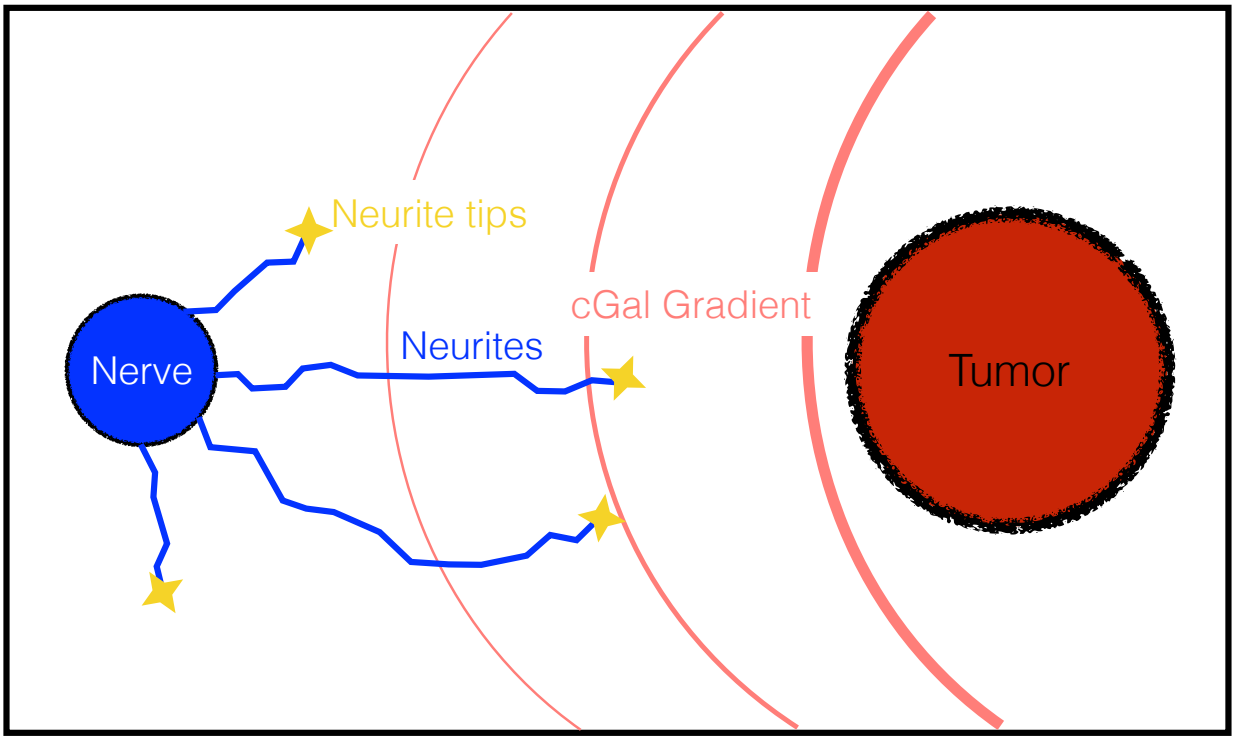

Figure 1: A pictorial representation of the model. The rough borders around the tumor and nerve represent secretion of gal by the tumor and nerve. The solid border around the edge represents no-flux boundary conditions. The neurites are shown growing out according to the directions chosen by their tips.

change directions at the tip in order to grow towards a signal (chemoattractants) or grow away from a signal (chemorepellent). Our model consists of a series of update rules for neurite tips. Growth is modelled by the movement of the tips, which is based on the biological phenomena outlined above. The movement algorithm is described below:

We consider the von Neumann neighborhood around a neurite tip. The first condition for chemotactic movement is that the amount of Gal at the tip's location is large enough that the tip can sense it. This is bounded below by the dissociation constant for the binding between Gal and its receptor: at low concentrations of Gal, very little Gal will be receptor-bound, and thus the signal will not be strong enough. We used the bound

$$0.01K_d < G \tag{2}$$

based on [12]. The next condition is that the gradient is sufficiently large for the neurite to sense. In particular, for neurites, the difference between Gal concentrations on two sides of the neurite arising from the gradient should be larger than the difference that could be expected to arise from noise. Based on work by Goodhill and Urbach, which simplifies estimates from Berg and Purcell, we used the bound

$$|(\nabla G)| > \sqrt{2}\Delta G_{noise} \tag{3}$$

where $|(\nabla G)|$ is the Gal gradient at a point and $\sqrt{2}\Delta G_{noise}$ an estimate of the RMS noise [13, 14]. If both the amount and the gradient of Gal are sufficient, then we consider the projections of the gradient vector, ∇G, onto the x- and y-axes. We weight the probability of moving horizontally (in the x-direction) and vertically (in the y-direction) as follows:

$$\begin{aligned} P_x &= \frac{\nabla G_x}{\nabla G_x + \nabla G_y} \\ P_y &= \frac{\nabla G_y}{\nabla G_x + \nabla G_y} \end{aligned} \tag{4}$$

provided that both spots are open/available for movement. If one spot is unavailable, then the neurite tips move to the available spot. If both spots are unavailable, then the neurite tip can move elsewhere with low probability.

In order to move randomly, we make the assumption that neurites have a directional "memory"

or inertia: they travel in the direction orthogonal or normal to the nerve cell body at the point where the neurite starts growing. This is based on the observation that neurites growing from dorsal root ganglia grow in a circular, radial pattern (similar to spokes from a hub) in the absence of external directional cues [15].

In the model, neurites have an angle associated with them, and the probability of moving in the x or y direction is associated with the cosine or sine of the angle, respectively. When neurites are initialised, the initial angle is defined. The angle can change when the gradient is sufficiently large, in which case the neurite's angle is changed to that of the gradient vector at that point. Movement is made with uniform probability, weighted by the angle as follows:

$$\begin{aligned} P_{x_1} &= \frac{k_1 \cos\theta}{\cos\theta + \sin\theta} \\ P_{y_1} &= \frac{k_1 \sin\theta}{\cos\theta + \sin\theta} \\ P_{x_2} &= \frac{(1-k_1)\cos\theta}{\cos\theta + \sin\theta} \\ P_{y_2} &= \frac{(1-k_1)\sin\theta}{\cos\theta + \sin\theta} \end{aligned} \tag{5}$$

where x_1 and y_1 represent the x and y directions away from the nerve body (i.e. extension), x_2 and y_2 represent the x and y directions away from the nerve body (i.e. retraction), and k_1 and $(1 - k_1)$ represent the probabilities of extension and retraction, respectively.

2.2 Model parameters

Model parameters were estimated based on literature values as indicated in the table.

The secretion rate of Gal by cancer was estimated based on literature values for Gal secretion [16]. Henson and co-authors estimate the amount of Gal secreted by 10^5 cells in 24 hours for various cancer cell lines [16]. By assuming simple secretion and decay of Gal, the instantaneous secretion rate per cell per hour was determined. The secretion rate of Gal by the nerve body is an order-of-magnitued estimate suggested by Goodhill [12]. The decay/degradation rate of Gal was estimated based on observations of the half-life of Gal in various tissues [17–19]. The diffusion constant was estimated using the method outlined by Goodhill [13], extrapolating the diffusion constant by assuming a direct relationship between the cube of the radius of a molecule and its

mass, and an inverse relationship between the diffusion constant and the radius of the molecule.

The time-step for neurite outgrowth is estimated at 3 minutes, based on the suggestion that neurites "integrate" signals on a time scale of 100 seconds [13], with additional time to represent the outgrowth of the neurite.

Table 1: Parameter values for the model.

Parameter	Definition	Units	Value	Sources
D	Diffusion constant of galanin	36 mm^2 hr^{-1}	0.02	Order-of-magnitude estimate after [13]
Γ_n	Secretion rate of nerve body	10^4 cells nM hr^{-1}	0.01093	order of magnitude estimate after [12]
Γ_c	Maximum secretion rate for tumor	nm hr^{-1}	4	fitted to data [16]
T	Time-step for neurite outgrowth	minutes	$\frac{10}{3}$	time-scale estimate from various sources
K_d	Dissociation constant of Gal binding to Gal receptors	nM	1-10	[20, 21]
a	Degradation/Decay rate of Gal	hr^{-1}	0.3781	fitted to data [17–19]

2.3 Data

The model output was compared visually to the phenotypes observed by Scanlon and co-authors in *in vivo* experiments [6], reproduced in Figure 2. The key feature is that with cancer cells that have Gal receptors (and thus can respond to Gal secreted by the nerve), there is significant neurite outgrowth from the nerve, in a directed fashion towards the cancer.

2.4 Chemoattractive regime

We define the chemoattractive regime at time t to be the set of points of the PDE domain such that the amount and gradient of Gal are sufficient for neurite tips to sense, that is, the set of points of the PDE domain that satisfies Equations 2 and 3 at time t. Since the chemoattractive regime is centered around the cancer cells, we define the chemoattractive regime radius to be the distance

between the center of the cancer cells and the point of the chemoattractive regime nearest where the nerve would be centered in our simulations (i.e. the left-most point of the chemoattractive regime). We also studied the chemoattractive regime in a simplified Gal submodel. In this model, we neglect the Gal secretion of the nerve; the boundary conditions are no-flux around the edge and non-zero-flux around the cancer cells. In this simplified model, we performed a sensitivity analysis by varying the diffusion constant (D), amount threshold ($0.01K_d$), and Gal secretion rate of cancer (Γ_c) and calculating the chemoattractive regime radius at 48 hours. We chose 48 hours because the chemoattractive regime appears to reach a steady state within a few hours (see Figure 5.

3 Results

3.1 Simulations with 0 tumor boundary condition

We first performed simulations with a no-flux boundary condition around the tumor, to represent a tumor that does not secrete Gal (in the experimental setup, this corresponds to the control cells). In this simulation, the neurites simply grew radially (Figure 3).

3.2 Simulations with non-zero tumor boundary condition

In these simulations, the tumor had non-zero flux boundary condition, representing a tumor that secretes Gal. In this simulation, the neurites grew radially initially, but by Day 3, showed an "inflection point", as they turned and grew directly towards the cancer (Figure 4).

3.3 Chemoattractive regime

These simulations show the size of the chemoattractive regime in the simplified model (Figure 5A). The chemoattractive regime radius quickly reaches a numerical steady state in the simplified model (Figure 5B), which justifies studying the steady-state behavior of the chemotactic regime in our sensitivity analysis.

3.4 Sensitivity analysis: chemoattractive regime

These simulations show the steady-state chemoattractive regime radius with respect to various parameters. Panel A and B of Figure 6 shows that the regime radius is insensitive to the amount

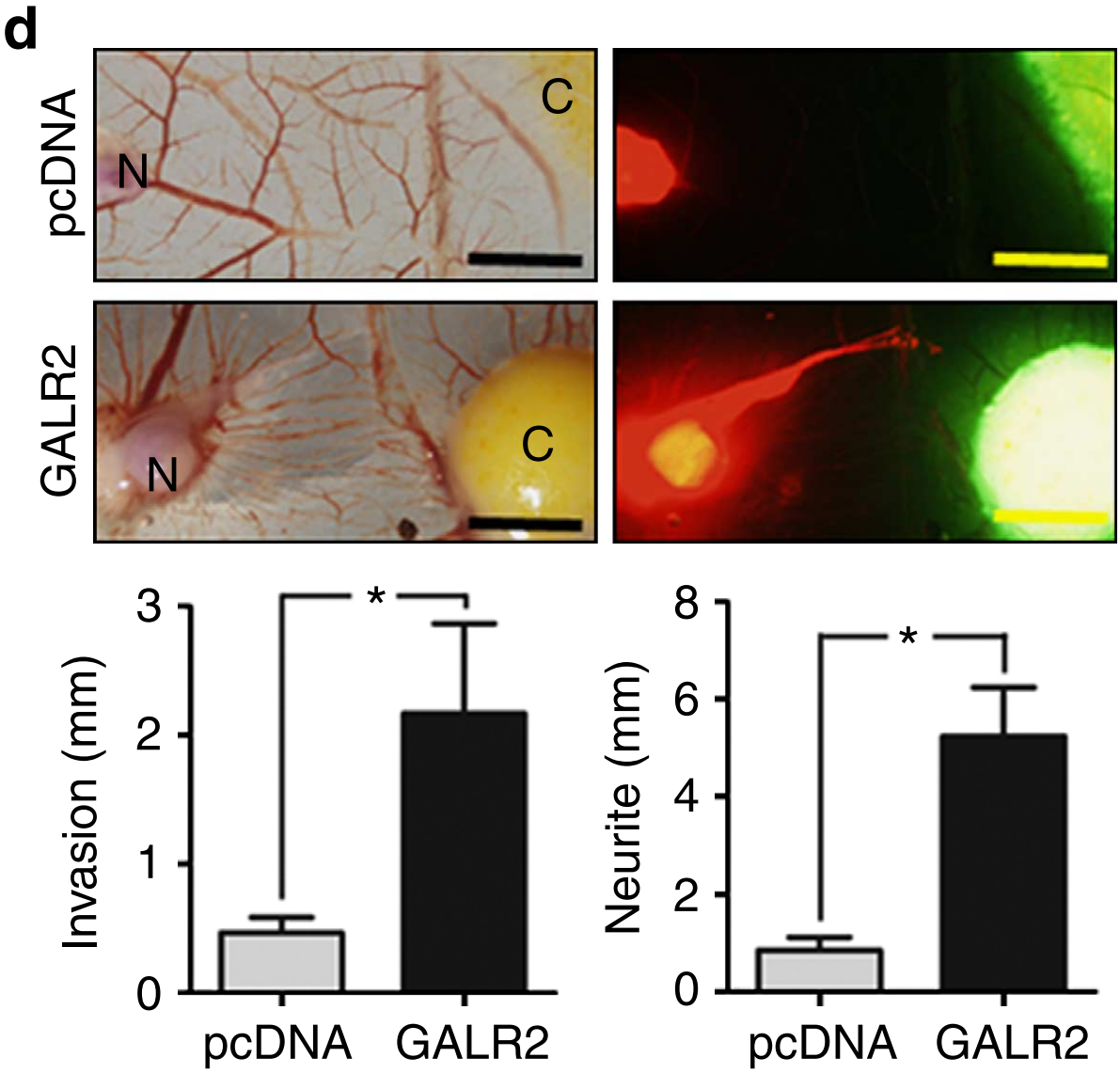

Figure 2: This figure shows neurite outgrowth from rat dorsal root ganglia (labeled N) co-cultured with tumor cells (labeled C) in the CAM experimental model system. The panels on the left are visible-light images; the panels on the right show the neurites labeled with a red fluorescent tag and the cancer labeled with a green fluorescent tag. The top row, labeled "pcDNA", represents cancer cells that do not have Gal receptor proteins, and thus are not induced by the dorsal root ganglion to secrete Gal. The second row, labeled "GalR2", represents cancer cells with Galanin receptor 2 (GalR2), which secrete Gal in response to the Gal from the dorsal root ganglion. Both invasion by the cancer and neurite outgrowth are significantly increased by the presence of GalR2-positive, Gal-secreting cancer cells. Reprinted from [6]. Reprinted with permission from the publishers.

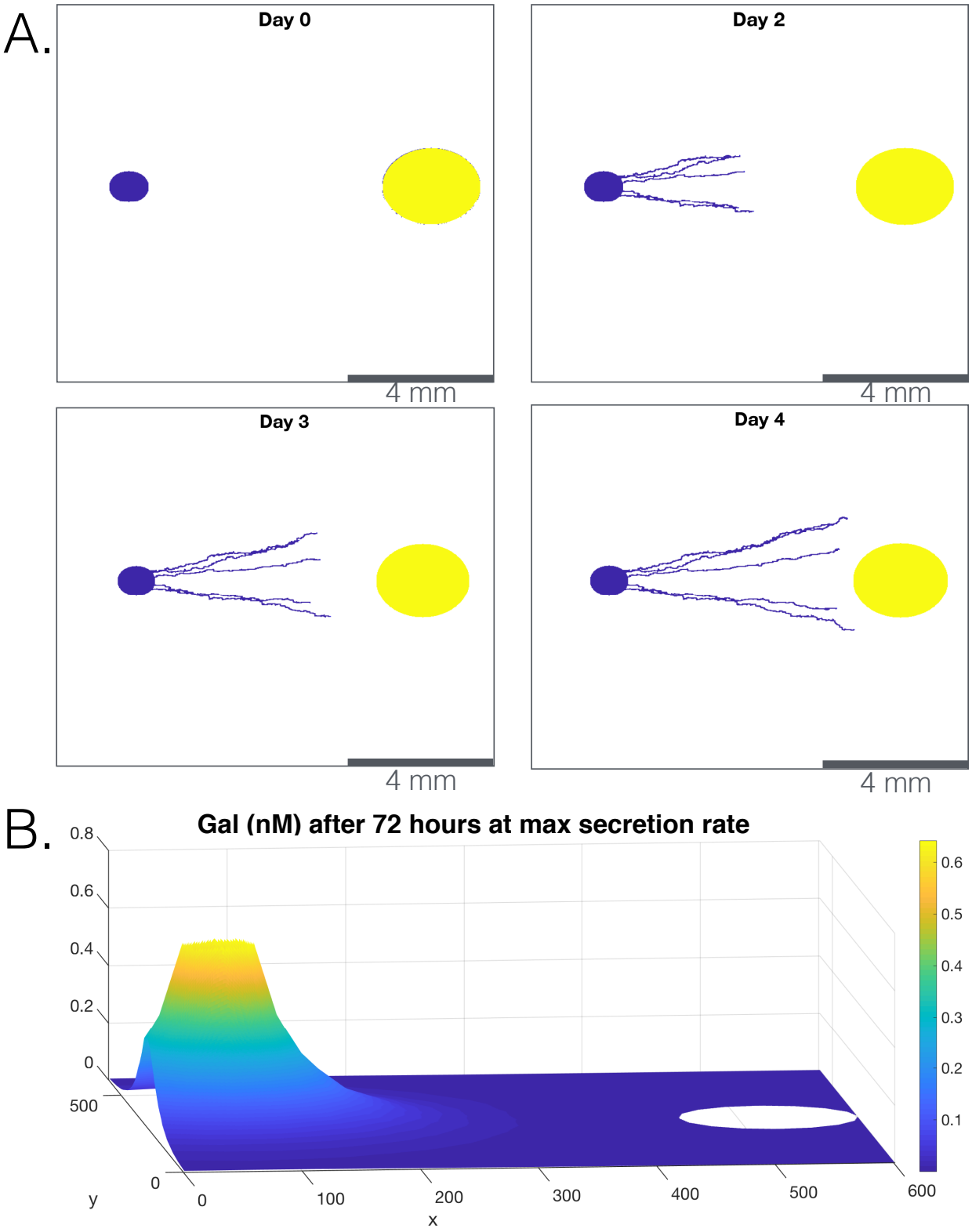

Figure 3: A. Simulations with tumor that does not secrete Gal. Cancer cells are depicted in yellow; nerve/neurites are depicted in blue. B. The gradient of Gal in the PDE domain (in nM). The nerve is the "hole" in the domain on the left; the cancer cells are represented by the "hole" the right. In these simulations, the cancer cells had a no-flux boundary condition to represent a 0 secretion rate.

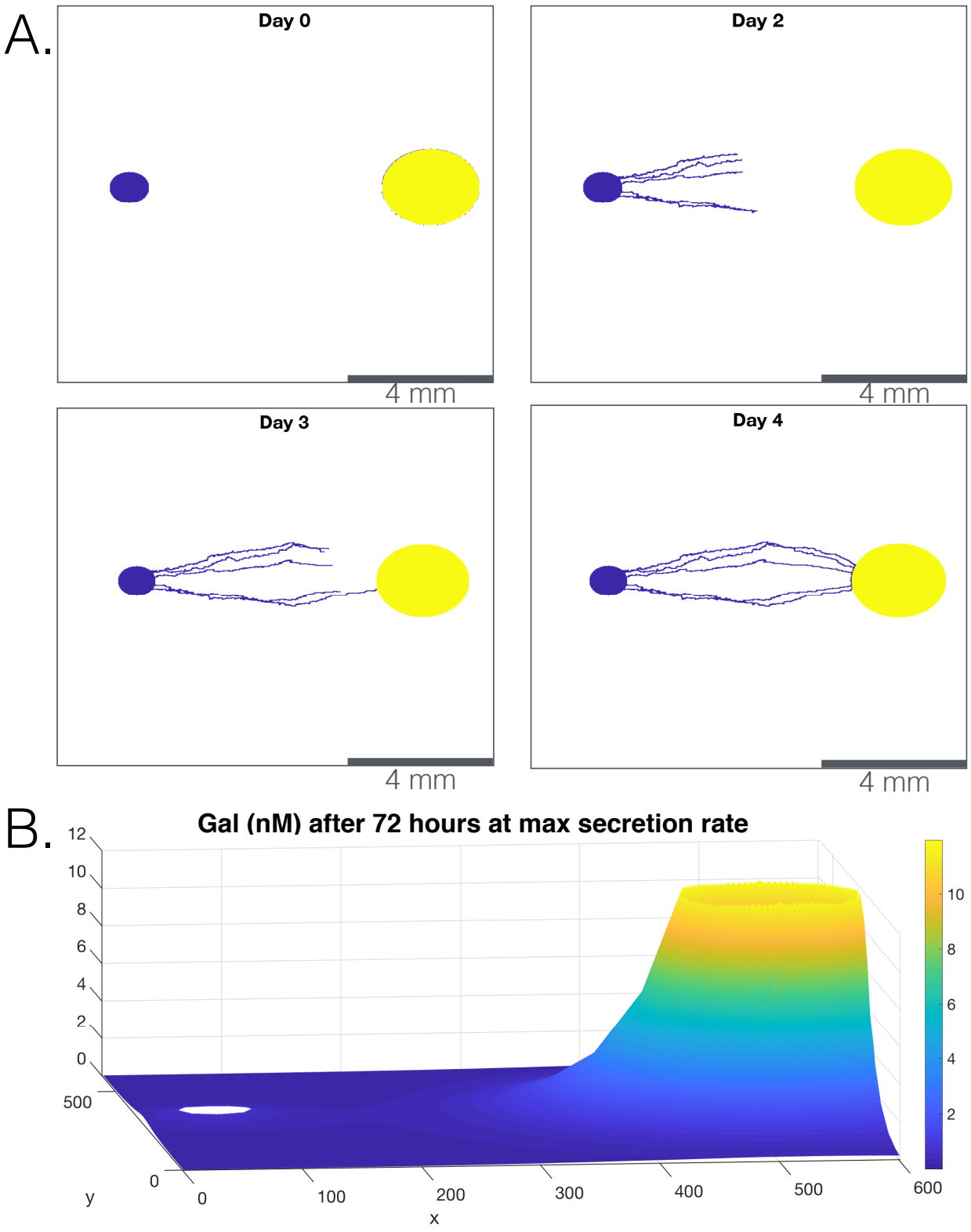

Figure 4: A. Simulations with tumor that secretes Gal (non-zero tumor boundary conditions). Cancer cells are depicted in yellow; nerve/neurites are depicted in blue. B. The gradient of Gal in the PDE domain (in nM). The nerve is the "hole" in the domain on the left; the cancer cells are represented by the "hole" the right.

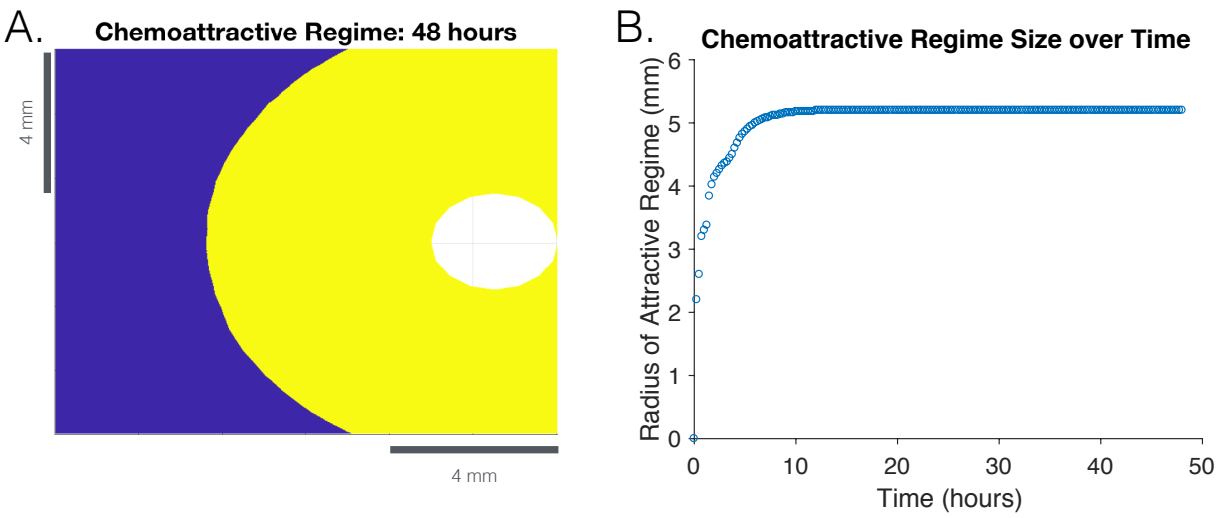

Figure 5: A. Plot of chemotactic regime in the simplified model. The regime is colored in yellow; points in the domain outside the chemotactic regime are coloured in violet. B. The radius (from the center of the cancer to the edge of the chemotactic regime)

threshold but sensitive to D, the diffusion constant of Gal, and Γ_c, the secretion rate of Gal by the tumor. In particular, increasing the diffusion constant leads to a larger chemoattractive regime, with a relationship that is approximately log-linear. Increasing secretion rate also leads to a larger chemoattractive regime. At low diffusion constants, the chemoattractive regime is insensitive to small in secretion rate above a non-zero secretion rate.

4 Discussion

4.1 Qualitative comparison of model and data

By accounting for known aspects of neurite outgrowth and of the biological mechanism of PNI, we successfully captured the overall phenotype of neurite outgrowth in the CAM model for PNI: random radial outgrowth followed by chemotactically directed outgrowth towards the tumor. Our results qualitatively match the experimental data in time-scale and distance scales.

One aspect of the experimental data in Figure 2 that the model fails to capture adequately is the observed polarisation of the neuron: there is one very large neurite or neurite bundle and a cloud of smaller neurites. Since the model does not contain any polarisation terms, the model fails to capture this effect.

Finally, the model simulations with 0 tumor boundary conditions show significant neurite out-

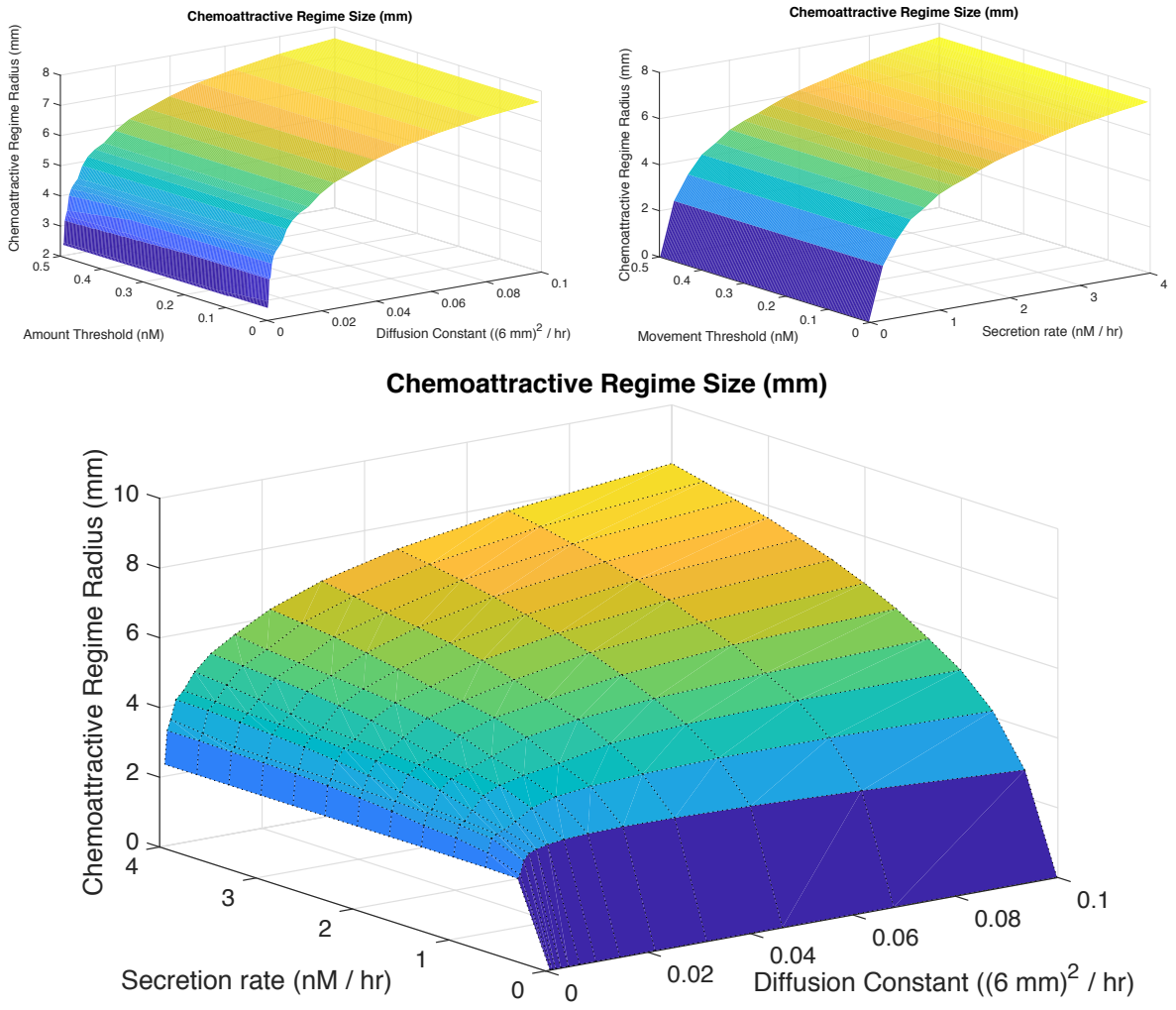

Figure 6: A. Chemoattractive regime radius with respect to diffusion constant (D) and amount threshold ($0.01K_d$). B. Chemoattractive regime radius with respect to secretion rate of cancer (Γ_c) and amount threshold($0.01K_d$). C. Cheomoattractive regime radius with respect to diffusion constant (D) secretion rate of cancer (Γ_c).

growth, unlike the control (top row) experimental results in Figure 2. This could potentially be overcome by rescaling the movement probabilities or diffusion constant, but it is worth noting that in its present form, the model does not account for the lack of neurite outgrowth seen in the case that the cancer does not secrete Gal.

4.2 Interpreting the chemoattractive regime

The chemotactic regime is defined to be the area around the cancer where the amount and gradient of Gal are large enough to direct neurite outgrowth towards the cancer. Our results suggest that the chemoattractive regime is large enough to attract neurites from >1 mm away (in the CAM model), but not always large enough to extend all the way to the nerve body (depending on the Gal secretion rate and the diffusion constant).

This suggests that both undirected and directed neurite outgrowth contribute to neurites growing towards cancer: random outgrowth allows neurites to reach the chemotactic regime, where they can grow in a directed fashion towards the tumor. This mechanism is consistent with experimental observations of PNI in the CAM model (Figure 2, unpublished observations), which show a certain amount of radial neurite outgrowth, with long enough neurites turning or bending towards the tumor. The concept of the chemotactic regime is a succinct encapsulation of these observations.

4.3 Limitations

The neurite submodel is a relatively simplistic, phenomenological approach to neurite outgrowth. The bounds for amount and gradient of Gal that a neurite can sense take the place of a more elaborate receptor model, and we do not incorporate the process of polarization into our model. As such, the neurite outgrowth trajectories are individually plausible, but it is unlikely that one DRG would send out 5 distinct neurites of similar length.

The tumor model is a mass/aggregate model: we do not consider the dynamics of individual cells. This is seen in two ways: first, we do not consider within-cell dynamics or intra-tumor dynamics in the secretion of Gal, and second, we do not consider invasive (i.e. moving) tumor cells. The first limitation could be overcome with a cellular model for the tumor, incorporating within-cell dynamics, proliferation, and other features of a tumor. The second limitation could be overcome by incorporating cancer cell motility (for a recent review of cancer models, see [7]).

Certain parameters need better estimation or fitting. The diffusion constant for Gal should be obtained experimentally in tissues, ideally by live imaging, since it is clear from Figure 6 that the diffusion constant determines the size of the chemoattractive regime. In addition, the assumption of pure Fickian diffusion may be inaccurate given that the presence of cells may interfere with diffusion (i.e. perhaps cellular transport should be considered). Imaging experiments with labeled Gal would potentially validate the assumption about diffusion or suggest a better model for Gal transport.

4.4 Future directions

This preliminary model offers several opportunities for mathematical extension as well as experimental validation.

4.4.1 Modeling

This model could be extended in several ways. It is known that extending a biological model from two spatial dimensions to three spatial dimensions can change the dynamics of the model; the CAM PNI assay is quite flat in the sense that the interacting components do so on a relatively thin section of tissue, so a two-spatial-dimensional model is a reasonable choice. However, in order to apply this model to HNSCC in humans, it might be important to consider three-spatial-dimensional models (if they do, in fact have different dynamics) to reflect the spatial complexity of tumors in humans. Therefore, a logical extension of this work would be to develop an analogous model in three spatial dimensions.

In this model, we consider a neurite outgrowth algorithm to make the neurite model. However, this model could be formalised into a biased random walk. A 2013 biased random walk model of chemotaxis by Jain and Jackson has the additional advantage of including chemokine-receptor binding dynamics explicitly [11]. It would at least be beneficial to compare our more phenomenological gradient and amount sensing limits to the graded response functions based on receptor activation in that paper [11], either to validate or to improve the approach taken here. Additionally, some simple polarization model, such as a positive-feedback loop between length and growth for the longest neurite, would help recapture the observed phenotype of one larger neurite/neurite bundle and several smaller neurites.

This model captures neurite outgrowth towards a tumor; an important extension of this model is capturing the growth of cancer cells towards the nerve. A model with motile invasive cells is an important extension of this model. It would facilitate the study of the relative contribution of neurite outgrowth and cancer invasion to PNI, and perhaps elucidate the mechanism by which neurite outgrowth facilitates cancer invasion into the nerve.

4.4.2 Further experimental study

While most model parameters were estimated with some basis in Gal-specific literature, the diffusion constant for Gal was not obtained directly; this can be rectified with experiments for estimating the diffusion constant for a protein. In addition, the dynamics (diffusion and transport) of Gal in tissues and cells could be estimated [22]. Finally, further models could consider diffusion in the case that Fickian diffusion assumptions break down: i.e. an anisotropic, "molecularly crowded" environement [23].

Additional experiments could be performed to test the accuracy of the estimates of the minimum amount and gradient of galanin that a neurite can sense. For instance, Rosoff and coauthors developed an assay in which controllable amounts and gradients of a molecule can be printed onto a gel, and then the response of neurites can be quantified [24]. Similar assays could be performed with controlled amounts and gradients of Gal to study in detail the response of neurites to various concentration patterns of Gal.

4.5 Conclusion

In summation, we developed a modeling approach to simulate chemical and spatial components of the nerve-cancer interaction. This simple hybrid captures several important features of PNI, most importantly, the combination of random and directed neurite outgrowth observed in the CAM experiments. This combination suggests the existence of a chemoattractive regime, within which neurites move chemoatactically due to the Gal secretion of the tumor. Outside of this chemoattractive regime, the neurites cannot "sense" the cancer, so random outgrowth is necessary to reach the regime. The size of the chemoattractive regime suggests that both undirected and directed neurite outgrowth contribute to PNI. This preliminary study indicates that extensions of this model would be fruitful in providing insights about PNI, especially in testing treatment

strategies.

References

[1] R. C. Inglehart, C. S. Scanlon, and N. J. DSilva, "Reviewing and reconsidering invasion assays in head and neck cancer," Oral oncology, vol. 50, no. 12, pp. 1137–1143, 2014.

[2] UICC, "Locally advanced squamous carcinoma of the head and neck," Union for International Cancer Control (UICC) 2014 Review of Cancer Medicines on the WHO List of Essential Medicines, 2014.

[3] J. Batsakis, "Nerves and neurotropic carcinomas.," The Annals of otology, rhinology, and laryngology, vol. 94, no. 4 Pt 1, pp. 426–427, 1985.

[4] C. Liebig, G. Ayala, J. A. Wilks, D. H. Berger, and D. Albo, "Perineural invasion in cancer," Cancer, vol. 115, no. 15, pp. 3379–3391, 2009.

[5] N. O. Binmadi and J. R. Basile, "Perineural invasion in oral squamous cell carcinoma: a discussion of significance and review of the literature," Oral oncology, vol. 47, no. 11, pp. 1005–1010, 2011.

[6] C. S. Scanlon, R. Banerjee, R. C. Inglehart, M. Liu, N. Russo, A. Hariharan, E. A. van Tubergen, S. L. Corson, I. A. Asangani, C. M. Mistretta, et al., "Galanin modulates the neural niche to favour perineural invasion in head and neck cancer," Nature communications, vol. 6, 2015.

[7] P. M. Altrock, L. L. Liu, and F. Michor, "The mathematics of cancer: integrating quantitative models," Nature Reviews Cancer, vol. 15, no. 12, pp. 730–745, 2015.

[8] M. Scianna, C. Bell, and L. Preziosi, "A review of mathematical models for the formation of vascular networks," Journal of theoretical biology, vol. 333, pp. 174–209, 2013.

[9] G. Lolas, A. Bianchi, and K. N. Syrigos, "Tumour-induced neoneurogenesis and perineural tumour growth: a mathematical approach," Scientific reports, vol. 6, 2016.

[10] A. L. Bauer, T. L. Jackson, and Y. Jiang, "A cell-based model exhibiting branching and anastomosis during tumor-induced angiogenesis," Biophysical journal, vol. 92, no. 9, pp. 3105–3121, 2007.

[11] H. V. Jain and T. L. Jackson, "A hybrid model of the role of vegf binding in endothelial cell migration and capillary formation," Frontiers in oncology, vol. 3, 2013.

[12] G. J. Goodhill, "Diffusion in axon guidance," European Journal of Neuroscience, vol. 9, no. 7, pp. 1414–1421, 1997.

[13] G. J. Goodhill, J. S. Urbach, et al., "Theoretical analysis of gradient detection by growth cones," Journal of neurobiology, vol. 41, no. 2, pp. 230–241, 1999.

[14] H. C. Berg and E. M. Purcell, "Physics of chemoreception," Biophysical journal, vol. 20, no. 2, pp. 193–219, 1977.

[15] J. Xie, M. R. MacEwan, X. Li, S. E. Sakiyama-Elbert, and Y. Xia, "Neurite outgrowth on nanofiber scaffolds with different orders, structures, and surface properties," ACS nano, vol. 3, no. 5, pp. 1151–1159, 2009.

[16] B. S. Henson, R. R. Neubig, I. Jang, T. Ogawa, Z. Zhang, T. E. Carey, and N. J. D'Silva, "Galanin receptor 1 has anti-proliferative effects in oral squamous cell carcinoma," Journal of Biological Chemistry, vol. 280, no. 24, pp. 22564–22571, 2005.

[17] K. Bedecs, Ü. Langel, and T. Bartfai, "Metabolism of galanin and galanin (1–16) in isolated cerebrospinal fluid and spinal cord membranes from rat," Neuropeptides, vol. 29, no. 3, pp. 137–143, 1995.

[18] K. Bedecs, M. Berthold, and T. Bartfai, "Galanin10 years with a neuroendocrine peptide," The international journal of biochemistry & cell biology, vol. 27, no. 4, pp. 337–349, 1995.

[19] T. Land, T. Bartfai, et al., "Hypothalamic degradation of galanin (1–29) and galanin (1–16): identification and characterization of the peptidolytic products," Brain research, vol. 558, no. 2, pp. 245–250, 1991.

[20] Y. Chen, A. Fournier, A. Couvineau, M. Laburthe, and B. Amiranoff, "Purification of a galanin receptor from pig brain.," Proceedings of the National Academy of Sciences, vol. 90, no. 9, pp. 3845–3849, 1993.

[21] C. K. Chen, T. McDonald, and E. Daniel, "Characterization of galanin receptor in canine small intestinal circular muscle synaptosomes," American Journal of Physiology-Gastrointestinal and Liver Physiology, vol. 266, no. 1, pp. G106–G112, 1994.

[22] E. A. Reits and J. J. Neefjes, "From fixed to frap: measuring protein mobility and activity in living cells," Nature cell biology, vol. 3, no. 6, pp. E145–E147, 2001.

[23] D. S. Banks and C. Fradin, "Anomalous diffusion of proteins due to molecular crowding," Biophysical journal, vol. 89, no. 5, pp. 2960–2971, 2005.

[24] W. J. Rosoff, J. S. Urbach, M. A. Esrick, R. G. McAllister, L. J. Richards, and G. J. Goodhill, "A new chemotaxis assay shows the extreme sensitivity of axons to molecular gradients," Nature neuroscience, vol. 7, no. 6, pp. 678–682, 2004.